Impact of Wetting and Drying Cycles on the Hydromechanical Properties of Soil and Implications on Slope Stability

Shah, Syed Samran Ali, Turrakheil, Kanishka and Naveed, Muhammad ORCID: https://orcid.org/0000-0002-0923-4976 (2024) Impact of Wetting and Drying Cycles on the Hydromechanical Properties of Soil and Implications on Slope Stability. Atmosphere, 15 (11). p. 1368.

This is the Published Version of the final output.

Article

Impact of Wetting and Drying Cycles on the Hydromechanical Properties of Soil and Implications on Slope Stability

Syed Samran Ali Shah [ID], Kanishka Sauis Turrakheil [ID] and Muhammad Naveed *

School of Computing and Engineering, University of West London, London W5 5RF, UK;
kanishka.turrakheil@uwl.ac.uk (K.S.T.)

* Correspondence: muhammad.naveed@uwl.ac.uk

Abstract: The soil-based infrastructure is the backbone of the global economy, connecting people, enhancing quality of life, and promoting health and safety. However, its vulnerabilities are becoming apparent due to climate change, mainly through frequent wetting and drying (wd) cycles. Despite few studies in the past, research showing the stability of flood embankments in the long term, incorporating the impact of wetting and drying cycles on the hydromechanical characteristics of soil, is scarce. This study aimed to assess the impact of controlled wd cycles on the hydromechanical properties of clay and silty sand soils and its implications for the stability of a typical flood embankment. Volumetric changes were monitored during the wd cycles. The soil water characteristic curve (SWCC), saturated hydraulic conductivity (k_{sat}), effective cohesion (c′), and effective angle of internal friction (ϕ′) were measured at 1 and 10 wd cycles. The results indicated that the 10 wd cycles decreased the saturated moisture content and resulted in a flatter SWCC compared to the 1 wd cycle for clayey soil. The k_{sat} value was also significantly higher at 10 wd cycles than 1 wd cycle for clayey soil. An insignificant difference was found in both the SWCC and k_{sat} at 1 and 10 wd cycles for silty sand soil. The ϕ′ value for the clayey soil decreased from 28.5 to 20.1 as the wd cycles increased from 1 to 10, while c′ remained unchanged at 10 kN/m². On the other hand, for the silty sand soil, ϕ′ increased from 34.6 to 37.5 with an increase in wd cycles from 1 to 10, and c′ remained constant at 1 kN/m². Numerical modelling of transient water flow coupled with a slope stability analysis revealed that the stability of a flood embankment depends on the evolution of soil hydromechanical properties due to wd cycles and the duration of flooding. These findings underscore the need for proactive measures to mitigate landslide risks in regions prone to frequent wd cycles, thereby ensuring the safety and resilience of slopes and associated infrastructure.

Keywords: wetting–drying cycles; soil water characteristics; saturated hydraulic conductivity; shear strength of soil; slope stability analysis

1. Introduction

Climate-related disasters, such as landslides, significantly threaten human well-being. They cause financial losses, harm to civil infrastructure, the disruption of daily life, and the potential for loss of life. Climate change is projected to worsen these issues by changing the seasonal pattern of wet and dry periods and increasing the severity of seasonal cycles [1,2]. Research in geotechnical and geological engineering has demonstrated that cyclic wetting and drying (wd) notably impacts soil hydromechanical properties, decreasing slope strength and durability. This phenomenon occurs when soil is directly exposed to the atmosphere during seasonal variations in precipitation and evapotranspiration [2]. Recent studies have emphasised the significant and irreversible structural damage caused by wd cycles in geomaterials. For instance, swelling minerals in soft soils during wetting and drying can lead to changes in volume and, ultimately, to desiccation cracking [3]. Past research has comprehended the effects of wd cycles on soils, indicating that wd cycles lead to cracks in the soil structure mainly due to the non-uniform growth in volumetric

strain [4]. Consequently, these cycles compromise the strength and stiffness of the soil and result in the progressive failure of earth structures [4–6].

During wd cycles, the soil's structure undergoes significant changes [1]. This manifests as two primary effects on the soil's characteristics. Firstly, it causes the soil's strength to deteriorate [5–9]. Secondly, it impacts soil water characteristics and hydraulic conductivity [10,11]. For example, research by Xu et al. [5] and Li et al. [6] examined the strength decay laws of expansive soils and clays under wd cycles. They all concluded that the soil cohesion would significantly decrease as the number of wd cycles increased. Gowthaman et al. [12] found that the unconfined compressive strength of soil treated with microbially produced calcium carbonate precipitation decreased with an increasing number of wd cycles. Additionally, Rasul et al. [13] observed that samples undergoing wd showed noticeably more permanent deformation and had lower robust modulus values than samples that did not undergo wd. During wd cycles, Stirling et al. [14] observed a dramatic reduction in deviator stress at failure. Several other studies [15,16] also yielded similar outcomes. Zhao et al. [16], using consolidated undrained triaxial tests, found that clayey soil's undrained elastic modulus, undrained shear strength, cohesion, and angle of internal friction decrease during wetting–drawing, freezing–thawing, and wetting–drawing/freezing–thawing cycles, with the reduction being most pronounced during the latter two.

The hydraulic characteristics of soil, including soil water characteristics and permeability, in addition to soil shear strength, play a crucial role in slope stability [14]. These characteristics are influenced by factors such as the soil particle size distribution, soil structure, and environmental elements like wetting–drying cycles, which can cause shrinkage, swelling, crack formation, and changes in the pore distribution [17–19]. Zhang et al. [17] investigated the soil water characteristic curve (SWCC) and saturated hydraulic conductivity of soil under different overlying stresses and wetting and drying cycles. Their findings revealed that wetting and drying cycles led to a decrease in the soil's saturated moisture content, an increase in the air-entry value, and a flatter SWCC. Moreover, the saturated hydraulic conductivity of the soil increased with an increase in the number of wetting and drying cycles. Ng and Daniel [18] observed decreased soil water holding capacity and hysteresis with an increasing number of wetting and drying cycles. Jing et al. [19] tested loess's SWCC and unsaturated permeability, explicitly considering the effect of wd cycles. They found lower water retention and higher unsaturated permeability with an increasing number of wd cycles. Wen et al. [20] reported that the size of the hysteresis loops decreases with an increase in the number of wd cycles, becoming almost identical after four. The estimated drying air-entry value decreases with the drying number and remains almost unchanged in the fourth and fifth drying cycles. While studying sandy clay derived from Durham lower boulder clay, Stirling et al. [14] found decreased deviator stress at failure and soil suction at a given water content with increasing wd cycles. While previous studies have focused on the influence of wetting and drying cycles on soil hydraulic characteristics, revealing their significant effects, only a limited number of studies have explored the impact of wd cycles on both the hydraulic and mechanical properties of soil simultaneously.

England and Wales have approximately 35,000 km of estuarine and river flood embankments. The annual budget for maintenance and new construction of these embankments is about GBP 450 million. These flood embankments must perform effectively during extreme flood events [21]. The long-term performance of flood embankments depends on the changes in the hydromechanical characteristics of soil with wetting and drying cycles. The stability of flood embankments during flooding events can be investigated using a combination of transient seepage and slope stability analyses, considering the time-dependent hydromechanical characteristics of soil [22]. Zhao [23] conducted numerical simulations coupling transient seepage and slope stability analysis to assess the effect of changes in soil strength and the hydraulic characteristics of soil with wd cycles. The study reported that the soil's strength parameter continuously deteriorates with an increased number of wetting–drying cycles, and the soil water characteristic curve exhibits a hysteresis effect.

The combination of these factors results in an overall decreasing trend of the slope safety factor, with a decrease of nearly 43%. Hassan et al. [24] conducted transient seepage and slope stability analyses using 2D finite element methods and time-history measurements on sandy and silty sand soils. They observed that fine particles increase the pore water pressure and reduce the factor of safety. Despite these few studies, research showing the performance of flood embankments in the long term, incorporating the impact of wetting and drying cycles on the hydromechanical characteristics of soil, is scarce. This study aims to conduct a comprehensive long-term stability analysis of a flood embankment model, focusing on the hydromechanical properties of fine-grained and coarse-grained soils. The analysis will involve an assessment of the impact of controlled wetting and drying cycles on the soil water characteristic curve, saturated hydraulic conductivity, and effective shear strength of the soil.

2. Materials and Methods

2.1. Preparation and Pre-Processing of Soil Samples

This study utilised two distinct soil types: fine-grained and coarse-grained soils. The fine-grained soil was sampled from Eynsham, Oxfordshire, United Kingdom (51°46′55″ N, 001°23′05″ W). The coarse-grained soil was sampled from Camden, London, United Kingdom (51°32′37″ N, 0°9′24″ W). Complying with BS 1377-1 [25], the soils were dried in an oven at 105 °C for at least 24 h to obtain the bulk soil. The soil was consistently turned throughout the drying process to prevent localised drying. The oven-dried soil was subsequently granulated and sieved through a 2 mm sieve, ready for testing. The soil particle size distribution was measured using wet-sieving and a hydrometer analysis [26]. The particle size distribution analysis of the fine-grained soil revealed a substantial clay content of 60%, accompanied by 37% silt and 3% sand. In contrast, the coarse-grained soil exhibited a lower clay content of 12%, along with 28% silt and a notably higher 60% sand content (Figure 1a). Meanwhile, the study encompassed the measurement of the soils' consistency limits, including their liquid limit, plastic limit, and plasticity index. The liquid and plastic limits were measured using the method outlined in BS 1377-2 [26]. The fine-grained soil demonstrated a liquid limit of 53% and a plastic limit of 22%, resulting in a plasticity index of 31. In comparison, the coarse-grained soil showcased a lower liquid limit of 32%, a plastic limit of 26%, and a smaller plasticity index of 7. As per the Unified Soil Classification System, the fine-grained soil was classified as CH, denoting clayey soil, and the coarse-grained soil as SM, representing silty sand. Standard Proctor compaction tests were conducted according to BS 1377-4 [27] to establish the relationship between the moisture content and dry density of the soil. The standard Proctor test results demonstrated that the clayey soil displayed a maximum dry density (MDD) of 1665 kg m^{-3} and an optimum moisture content (OMC) of 18%, whereas the silty sand exhibited values of 1686 kg m^{-3} and 17.6%, respectively (Figure 1b).

A total of 12 soil samples were prepared, with 6 samples for each type of soil at 90% of the maximum dry density and optimum moisture content. Each soil sample had a diameter of 50 mm and a height of 100 mm, and they were prepared using a split stainless-steel mould. The samples were compressed into four layers within the mould using the jack to achieve the required dry density. After compaction, the samples were removed from the mould and placed in sealed plastic bags covered with plastic films for 48 h at a room temperature of 25 ± 1 °C to reach moisture equilibrium. The soil samples' preparation and pre-processing are shown in Figure 2.
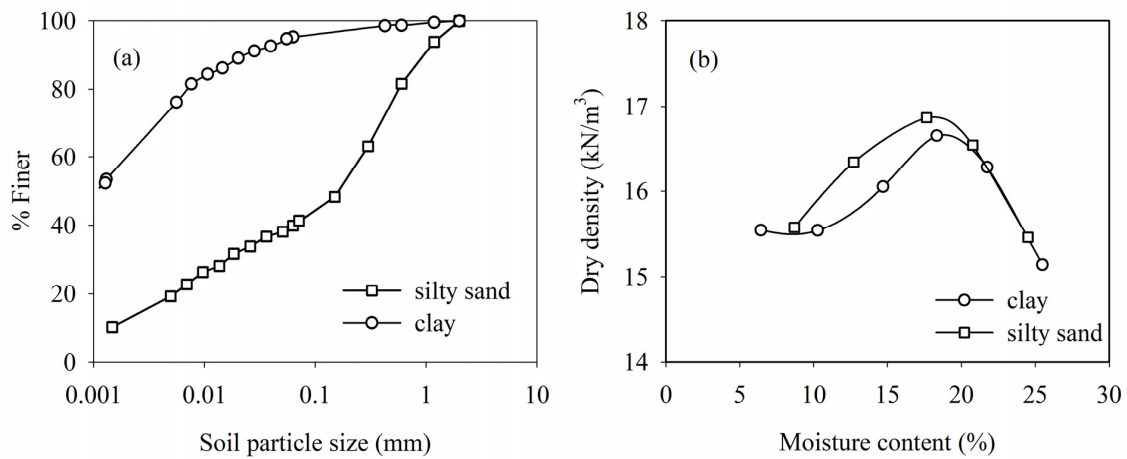
Figure 1. (**a**) Soil particle size distribution and (**b**) soil compaction characteristics.
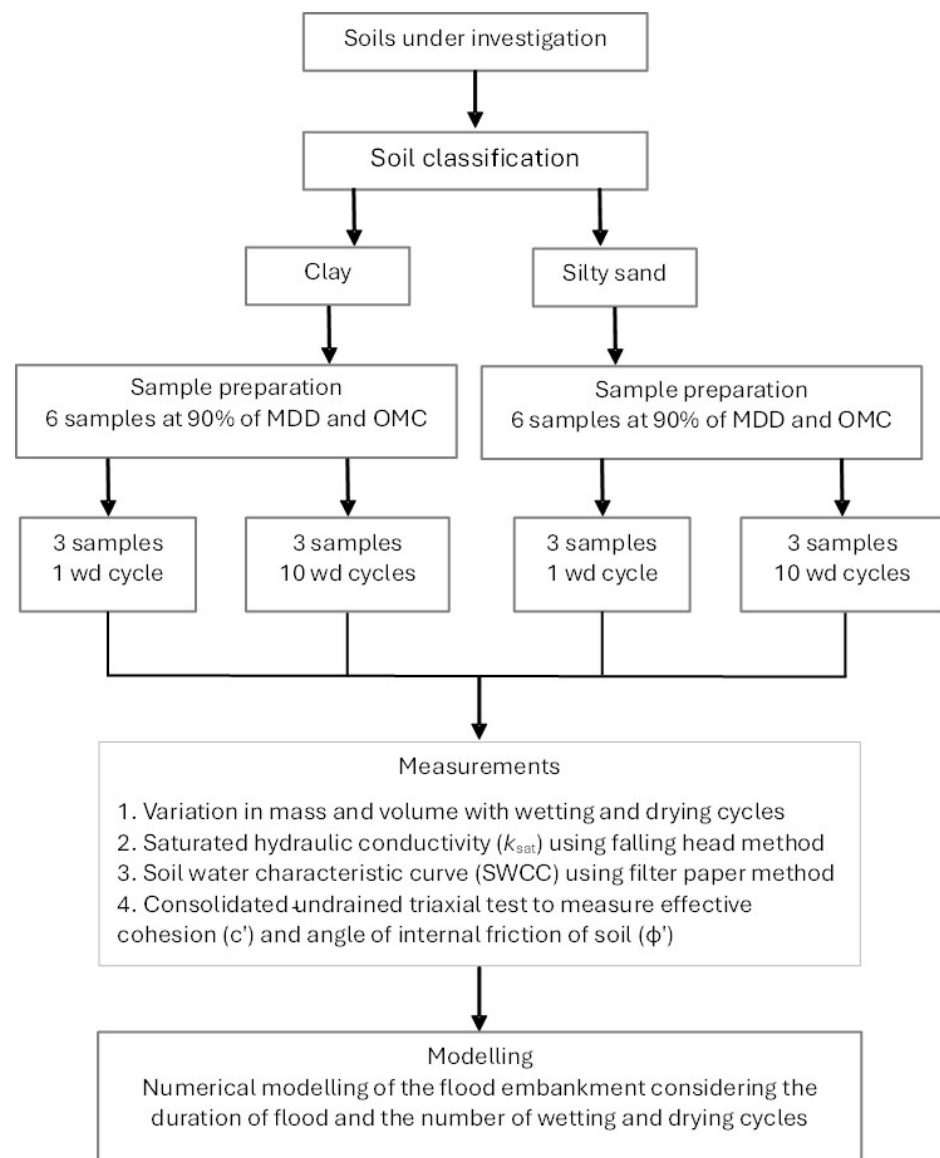

Figure 2. The study's flow chart. MDD, maximum dry density; OMC, optimum moisture content; wd, wetting and drying.

2.2. Application of Wetting and Drying Cycles

The clay and silty sand samples were divided into two sets of three. One set underwent a single wetting and drying cycle, while the other set underwent ten cycles, as indicated in Figure 2. Throughout the wetting and drying cycles, continuous monitoring was conducted to observe changes in volume and mass. The soil samples were saturated by enveloping them in a rubber membrane, placing them in a split plastic core, and leaving the top exposed while resting the bottom on a porous stone for soaking. The soil samples were enclosed in a split plastic core to safeguard them from damage and free swelling during saturation. The saturation process involved immersing half of the samples in water to facilitate capillary rise. The samples were kept saturated until the rate of sample weight change became negligible, typically taking an average of 5 days. Following saturation, the soil samples were extracted from the split plastic cores and stored for 48 h in sealed plastic bags at a room temperature of 25 ± 1 °C to achieve moisture equilibrium. Subsequently, the soil samples were dried at 25 °C, with each drying cycle typically lasting 5 to 6 days. The dried soil samples were again stored in sealed plastic bags for 48 h at 25 ± 1 °C to ensure moisture equilibrium. It is important to note that oven drying, commonly used in previous research, was avoided for soil drying due to the potential for sample cracking.

2.3. Measurement of Volumetric Change

The volumetric behaviour during the wd cycles was analysed by conducting volume measurements on soil samples after each cycle. These were measured on the specimens using an electronic Vernier calliper with an accuracy of 0.005 mm. Measurements of the specimens' diameter (i.e., d_1, d_2, and d_3) and height (i.e., h_1, h_2, and h_3) were made at three separate cross-sections evenly spaced on their surface. The measurements were made gently and carefully to avoid disturbing the specimens, particularly the fragile and damp ones on saturation. The volume of the specimens and the volumetric strain (ε_v) for each wd cycle were calculated using the average diameter and height measurement values. Using Equation (1), the specimens' volumetric strain (ε_v) was computed:

$$\varepsilon_v = (V_N - V_0)/V_0 \times 100\% \tag{1}$$

where V_0 is the initial volume of the specimen and V_N is the volume of the specimen after N cycles of wetting and drying. Positive ε_v indicates swelling, while negative ε_v refers to shrinkage.

2.4. Measurement of Saturated Hydraulic Conductivity (k_{sat})

To measure the saturated hydraulic conductivity of the soil samples after the required wetting and drying treatment, the falling head method was applied following BS 1377-6:1990 [28]. A fully saturated soil sample was placed in a permeameter and securely connected to a standpipe filled with water. The initial water head (h_0) was recorded at the start. The valve was then opened to allow water to flow through the soil sample, and the timer was started. The water head (h_1) was measured at regular intervals until it dropped to a lower level (h_2), and the time taken for this change was recorded. The length (L) and cross-sectional area (A) of the soil sample, along with the cross-sectional area of the standpipe (A_s), were measured. Using these measurements, the saturated hydraulic conductivity (k_{sat}) was calculated using the following formula:

$$k_{sat} = \frac{A_s L}{At} ln\left(\frac{h_0}{h_2}\right) \tag{2}$$

To ensure accuracy, the test was repeated three times for each soil sample, and the results were averaged, thus obtaining a reliable measurement of the soil's saturated hydraulic conductivity.

2.5. Measurement of Soil Water Characteristic Curve (SWCC)

After the measurement of k_{sat}, the soil water characteristic curves (SWCCs) were measured using the Whatman Grade 42 filter paper method. The filter paper was attached to each end of the sample, and then the sample was wrapped in a PVC film and aluminium foil to avoid the loss of its moisture content. The samples were placed in a desiccator for one week to equalise the sample's moisture and the filter paper. ASTM D-5298-93 [29], which stipulates seven days of storage as being necessary for moisture stabilisation between soil and paper, served as the basis for the time the samples were kept covered in PVC film and aluminium foil. After a week, the filter paper was removed from the sample and weighed precisely on an enclosed analytical balance to one ten-thousandth of a gram. The entire procedure was performed in 3 to 5 s [29]. The filter paper was then dried in an oven. This whole procedure was repeated for different moisture contents of the sample. For a metric potential equal to zero, the saturated moisture was used, calculated by the indirect method for porosity, given by Equation (3):

$$\theta_s = 1 - \frac{\gamma_s}{\gamma_p} \tag{3}$$

where θ_s is the saturated moisture content, and γ_s and γ_p are soil bulk and particle density, respectively.

Calibration curves for Whatman Grade 42 filter paper are frequently employed to calculate the value of matric suction, as given by Equations (4) and (5) [30]:

$$\text{For u} > 47\% \ \psi = 10^{(6.05 - 2.48\,\log(u))} \tag{4}$$

$$\text{For u} \leq 47\% \ \psi = 10^{(4.84 - 0.0622u)} \tag{5}$$

where the matric potential (ψ) in kPa is estimated by the correlation with the moisture content of the filter paper (u).

The measured SWCCs were fitted with the van Genuchten model [31].

2.6. Measurement of Effective Shear Strength of Soil

After the soil water characteristic curve (SWCC) measurements were conducted, the samples underwent testing in a triaxial cell under consolidated undrained (CU) conditions. Cell pressures of 50, 100, and 200 kPa were selected for each wetting and drying treatment to assess the effective shear strength parameters. It is crucial to emphasise that how the specimen is positioned within the triaxial cell significantly influences test outcomes. The correct alignment and preparation of the specimen are pivotal in ensuring precise and representative measurements. The mounting procedure directly influences factors such as the stress distribution, boundary conditions, and specimen's reaction to loading. Any errors or deficiencies during specimen installation may introduce stress concentrations, boundary effects, and a non-uniform stress distribution, ultimately distorting the observed response. Therefore, meticulous care must be taken to align the specimen, achieve proper saturation, and apply appropriate confining pressure to minimise such effects and obtain reliable and representative results in triaxial testing [32]. Initially, the samples were saturated in the triaxial cell to reach a B value of $\geq$0.95. The B value is defined as

$$B = \frac{\Delta u}{\Delta \sigma_c} \tag{6}$$

where Δu is the change in pore water pressure and $\Delta \sigma_c$ is the change in cell pressure.

After reaching full saturation, the specimens were consolidated by maintaining a uniform back pressure (BP) and increasing the cell pressure (CP) until the difference between the CP and BP equalled the desired consolidation pressure. The samples underwent isotropic consolidation at the required confining pressure. Subsequently, the consolidated samples were subjected to an undrained shearing stage. The samples were sheared until

the axial strain reached 20% under a 0.01 mm/min shearing rate. The Mohr–Coulomb failure criteria were employed using the peak values of deviator stress to calculate the effective cohesion and angle of internal friction of the soil.

2.7. Evaluating the Performance of Flood Embankment

The evaluation of the flood embankment's performance under wetting and drying cycles at various flood durations involved the utilisation of the "Slope Stability—Water Flow" modules within GEO5 (version 2018.31 (9.0)) software. GEO5 is a comprehensive software package that offers solutions for a wide range of tasks, spanning from geological surveys to advanced geotechnical design. The Water Flow module facilitates the determination of pore water pressures in the embankment slope through steady-state or transient groundwater seepage analysis using the finite element method. The computed pore water pressures were subsequently imported into the Slope Stability module to assess the factor of safety of the flood embankment based on Limit Equilibrium Methods (LEMs).

Figure 3 illustrates the flood embankment's geometry. The analysis adopted 3-node triangular elements with an edge length of 0.25 m. Given the embankment geometry, computation time, and accuracy of the output, no further mesh refinement was required. The initial, final, and boundary conditions are provided in Table 1. Input parameters such as the SWCC's van Genuchten model [31] parameters, initial void ratio, and k_{sat} are given in Table 2. Pore water pressures were calculated before and after flooding at 1, 5, and 30 days by utilising transient water flow analysis based on Richard's general equation (Equation (7)):

$$n.\dot{S} + div(-k_r k_{sat} \nabla h) = 0 \tag{7}$$

where n is the porosity, $\dot{S}$ is the rate of change of the degree of saturation, k_r is the coefficient of relative permeability, k_{sat} is the saturated hydraulic conductivity, and ∇h is the gradient of the total head.
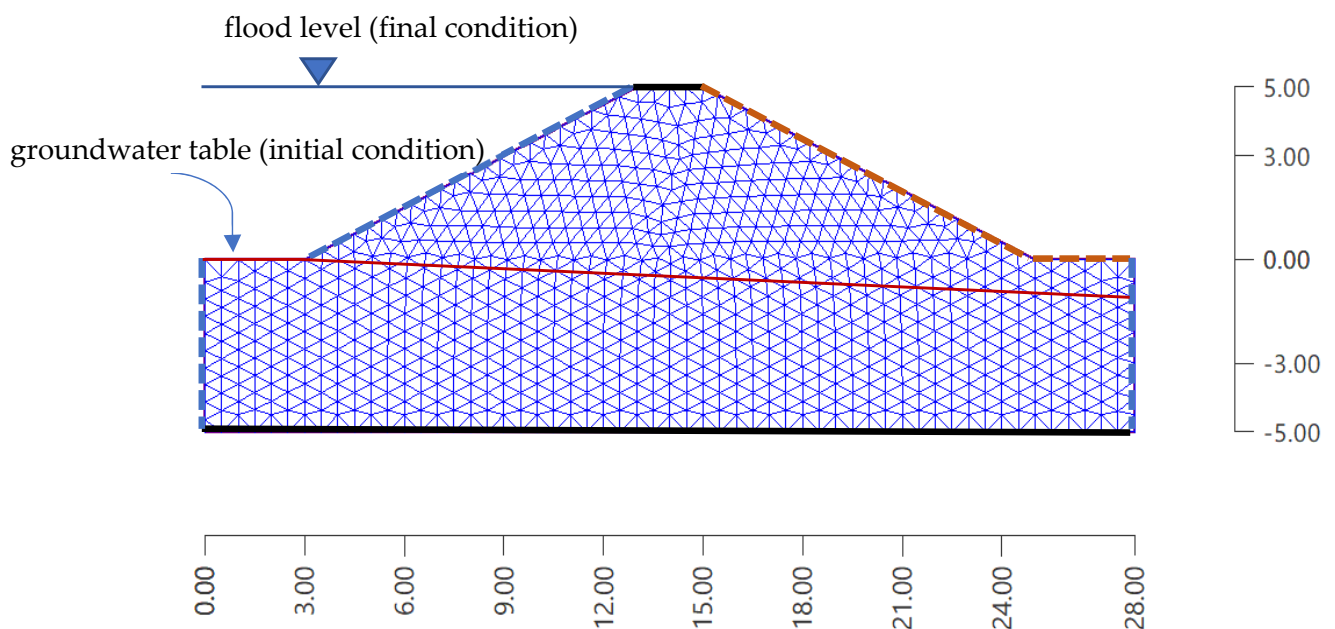

Figure 3. Flood embankment used for modelling; for the horizontal and vertical axes, the unit is meters. Solid red line shows water table, solid black line shows impermeable surfaces and dash red and blue lines shows seepage surfaces as given in Table 1.

Table 1. Initial, final, and boundary conditions for transient water flow analysis.

Initial Condition	Final Condition	Boundary Conditions
The groundwater table is shown in Figure 3.	Flood level to the crest of the embankment, as shown in Figure 3.	• Upstream face: pore pressure type with flood level of 5 m above the terrain surface • Downstream slope face: seepage type • Downstream horizontal face: seepage type • Downstream vertical face: groundwater table of −1 m below the terrain surface • Bottom boundary: impermeable • Embankment crest: impermeable

Table 2. Hydromechanical characteristics of soils.

Parameter	Clay		Silty Sand	
	1 wd Cycle	10 wd Cycles	1 wd Cycle	10 wd Cycles
dry density (kN/m^3)	16.2	16.2	16	16
saturated density (kN/m^3)	18.5	18.5	18	18
initial void ratio	0.67	0.67	0.66	0.65
effective angle of internal friction (deg.)	28.5	20.1	34.6	37.5
effective cohesion (kN/m^2)	10	10	1	1
saturated hydraulic conductivity (m/d)	0.0051	0.0331	1.061	1.032
van Genuchten parameter, α (1/m)	0.5	0.45	4.5	4.5
van Genuchten parameter, n (-)	1.25	1.19	1.84	1.77
saturated moisture content (m^3/m^3)	0.46	0.43	0.41	0.40

The time discretisation of Richard's equation is based on a fully explicit Picard's iteration scheme. This corresponds to a hybrid formulation ensuring the conservation of mass. The analysis was performed incrementally due to it being the solution of a generally nonlinear problem. The Standard Newton–Raphson iteration scheme was used to satisfy equilibrium conditions.

Subsequently, the "Slope Stability" module computed the embankment's factor of safety (FOS) using Bishop's method, taking into account the unit weight of soil, the effective cohesion, the effective angle of internal friction of soil as given in Table 2, and the pore water pressures calculated in the "Water Flow" module.

3. Results

3.1. Volumetric Behaviour of Soils Under Wetting and Drying Cycles

The saturated moisture content for clayey soil was found in the range of 23 to 25%, which is significantly higher than that for silty sand, around 18%. For the drying stage, the moisture content for clayey soil was targeted at 12%, whereas for silty sand, it was 5%. This is equivalent to a matric suction of −1500 kPa (wilting point). Under the drying condition, the volumetric strain varied between −7 and 11% for clayey soil, whereas it only fluctuated between −1 and 5% during wetting and drying cycles for silty sand. These findings illustrate the notable shrinkage and swelling of the clay soil samples during wetting and drying (wd) cycles, while the silty sand exhibited less pronounced changes in volume (Figure 4).
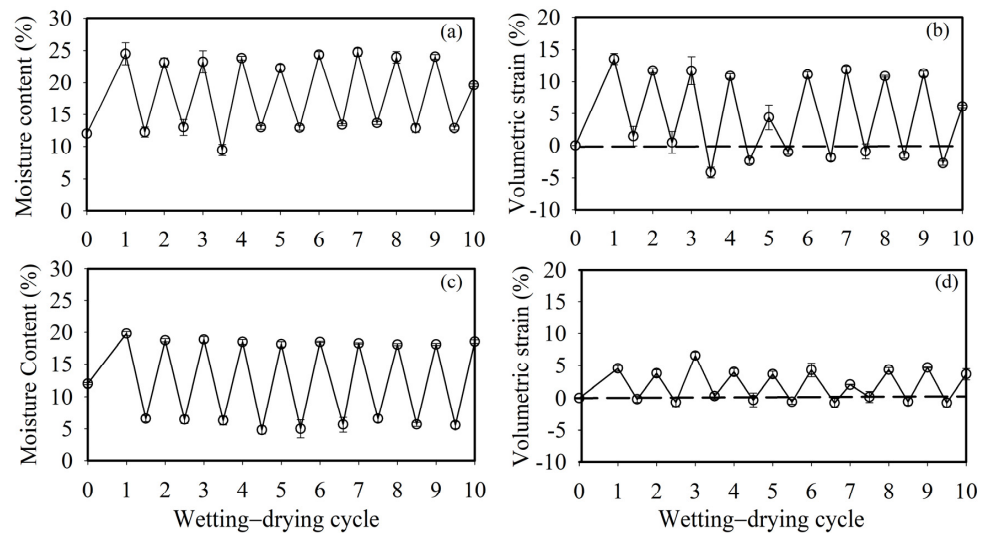
Figure 4. The average (**a**) moisture content of clayey soil, (**b**) volumetric strain of clayey soil, (**c**) moisture content of silty sand, and (**d**) volumetric strain of silty sand plotted as a function of wetting and drying cycles for the three replicates subjected to 10 wetting and drying cycles.

3.2. Hydraulic Characteristics of Soils Under Wetting and Drying Cycles

The clayey soil's average saturated hydraulic conductivity (k_{sat}) at one wd cycle was measured as 0.0051 m/day (m/d). Following 10 wd cycles, this value significantly increased to 0.0331 m/d. The average k_{sat} was measured for silty sand soil as 1.061 and 1.032 m/d at 1 and 10 wd cycles, respectively. The difference in k_{sat} values between replicates was negligible at one wd cycle for both the clay and silty sand soils. However, at 10 wd cycles, the dispersion in k_{sat} data for clayey soil was higher than that for silty sand soil. The measured soil water characteristic curves (SWCCs)—the average for three soil samples per treatment—are shown in Figure 5. The saturated moisture content for the clayey soil at 10 wd cycles was significantly lower than that at 1 wd cycle. However, this difference was reduced with increasing suction. The measured soil water characteristic curves for silty sand soil were similar, irrespective of wetting and drying treatments (Figure 5). The van Genuchten model [30] parameters for the fitted soil water characteristic curves are given in Table 1.
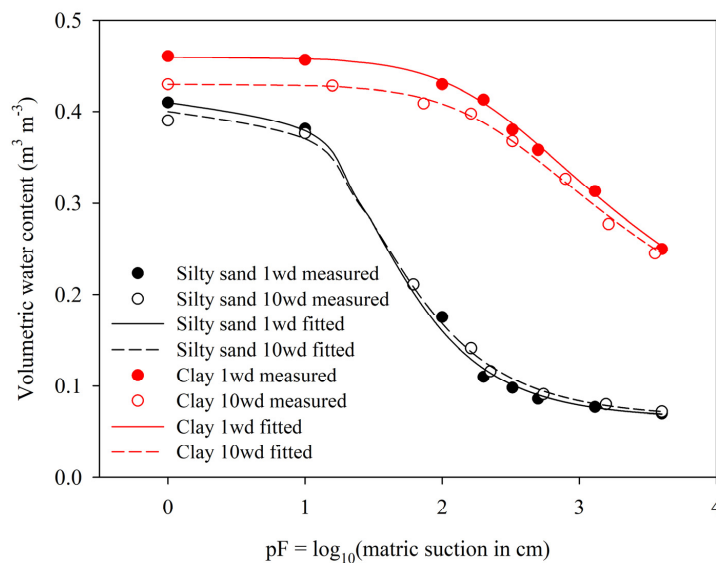

Figure 5. The measured soil water characteristic curves (SWCCs) for soils treated with 1 and 10 wetting and drying cycles.

3.3. Shear Strength of Soil Under Wetting and Drying Cycles

Figure 6 illustrates the deviator stress as a function of axial strain under confining pressures of 50, 100, and 200 kPa for both clayey and silty sand soils. The peak deviator stress increased with increasing applied confining pressure. The stress–strain responses for the clayey soil demonstrated strain-hardening behaviour, while the behaviour for the silty sand soil was characterised by strain-softening. Notably, the peak deviator stress values for the clayey soil after one wetting and drying cycle were 102, 159, and 207 kPa under cell pressures of 50, 100, and 200 kPa, respectively. Following 10 wetting and drying cycles, the peak deviator stress decreased to 70, 112, and 135 kPa, indicating soil deterioration due to the increased number of wetting and drying cycles. Additionally, the variation in the deviator stress for silty sand is represented in Figure 6d–f. The peak deviator stress values for the silty sand after one wetting and drying cycle were 121, 176, and 202 kPa under cell pressures of 50, 100, and 200 kPa, respectively. After 10 wetting and drying cycles, these values increased slightly to 143, 180, and 215 kPa, respectively.
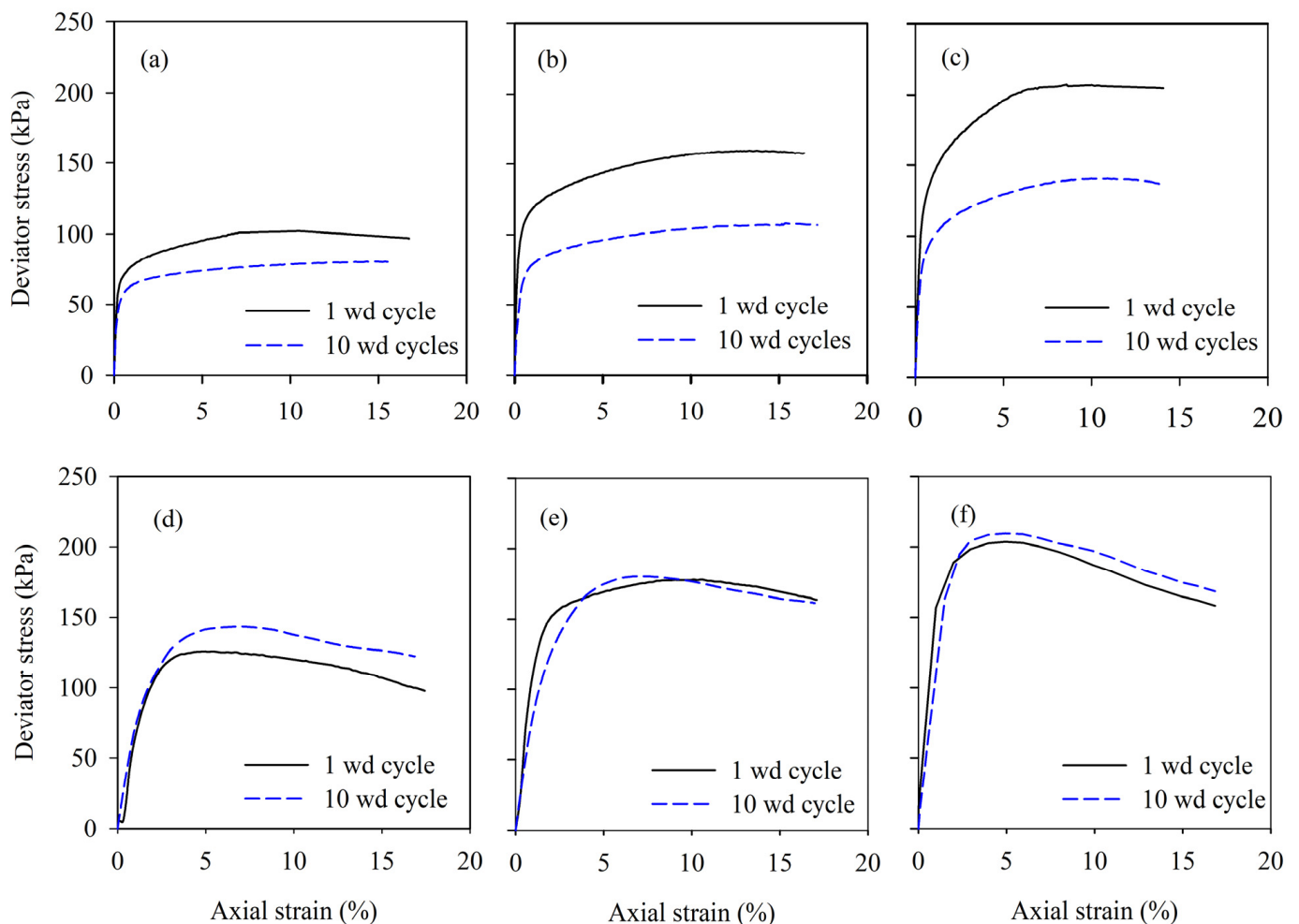

Figure 6. Deviator stress (kPa) plotted as a function of axial strain (%) measured using consolidated undrained triaxial tests for different numbers of wetting and drying (wd) cycles under various cell pressures: (**a**) clay 50 kPa, (**b**) clay 100 kPa, (**c**) clay 200 kPa, (**d**) silty sand 50 kPa, (**e**) silty sand 100 kPa, and (**f**) silty sand 200 kPa.

As shown in Figure 7, the results indicated that the effective cohesion of clayey soil was 10 kPa, which did not change with the number of wd cycles. However, the effective angle of internal friction decreased, with values ranging from 28.5 degrees at the onset to approximately 20.1 degrees after 10 wetting and drying cycles, representing a 29% reduction

in the soil's internal friction angle. In contrast, the effective cohesion for silty sand was 1 kPa, while the effective angle of internal friction increased from 34.6 to 37.5 degrees over 10 wetting and drying cycles. These fluctuations underscore the dynamic nature of soil behaviour in response to changes in moisture content, impacting its stability and resistance to deformation across successive wetting and drying cycles. A comprehensive understanding of these variations is essential for predicting and managing potential soil instability issues in engineering and construction applications.
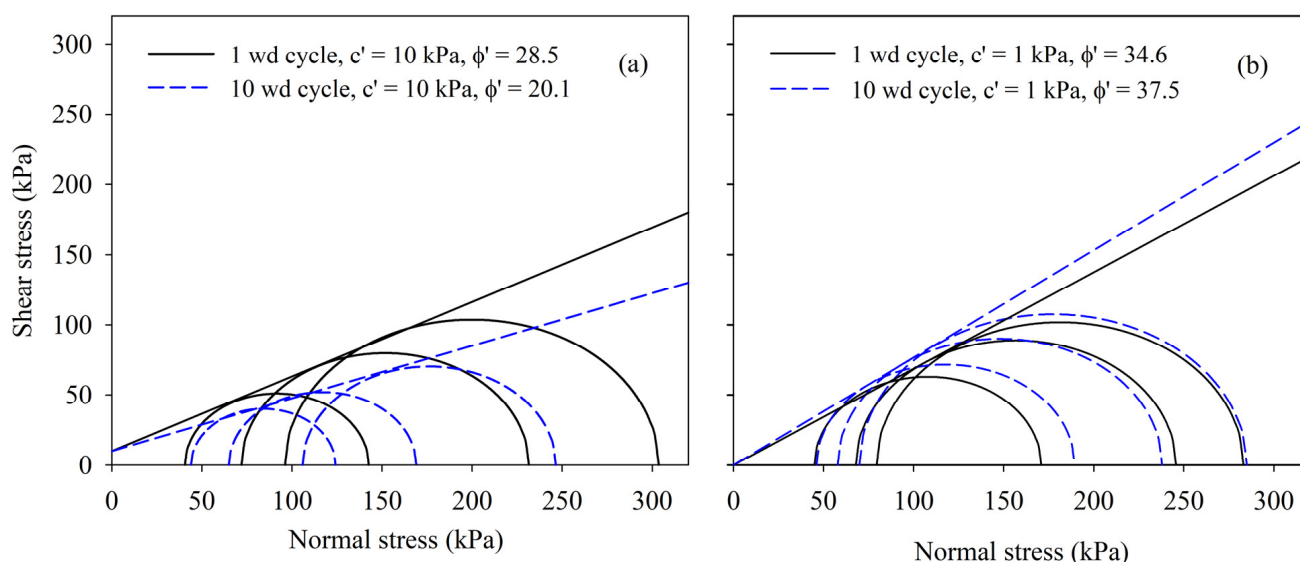

Figure 7. Mohr–Coulomb failure circles for (**a**) clay and (**b**) silty sand soils at 1 and 10 wd cycles.

3.4. Performance of Model Flood Embankment Under Wetting and Drying Cycles

Regardless of the number of wd cycles, the clay embankment exhibited impervious behaviour, as evidenced by the small inflow and outflow values in Table 3. The phreatic line for the clayey embankment extended to the downstream vertical face for all flooding durations. Therefore, there was no water discharge calculated at the seepage surface. Steady-state water flow was not achieved during the 10 days of flooding, as indicated by the significantly higher inflow than the outflow (Table 3). In the case of the silty sand embankment, water infiltration occurred relatively quickly, and equilibrium between the inflow and outflow (steady-state conditions) was reached after 10 days of flooding. The outflow consisted of water flowing from the seepage surface and downstream horizontal and vertical faces (Table 3).

The initial factor of safety for a newly constructed clayey embankment was determined to be 2.47. The duration of flooding to the crest level on days 1, 5, and 10 did not significantly impact the factor of safety of the newly constructed embankment due to the relatively impervious nature of the clayey soil (Table 3). Following exposure to 10 wetting and drying cycles, the factor of safety of the aged clayey embankment was measured at 1.99 before flooding, indicating a 20% reduction compared to the newly constructed embankment. Subsequently, with 5 days of flooding, the factor of safety of the aged clay embankment decreased to 1.72 (Table 3). Finally, with 10 days of flooding to the crest level, the factor of safety of the clay embankment exposed to 10 wd cycles was further reduced to 1.64, reflecting a 34% reduction in total (Figure 8). This decline is attributed to the loss of shear strength, soil suction, and increased saturated hydraulic conductivity of the soil due to wetting and drying cycles.

Table 3. Amount of water entering and exiting for a particular duration of infiltration and factor of safety of the corresponding embankment.

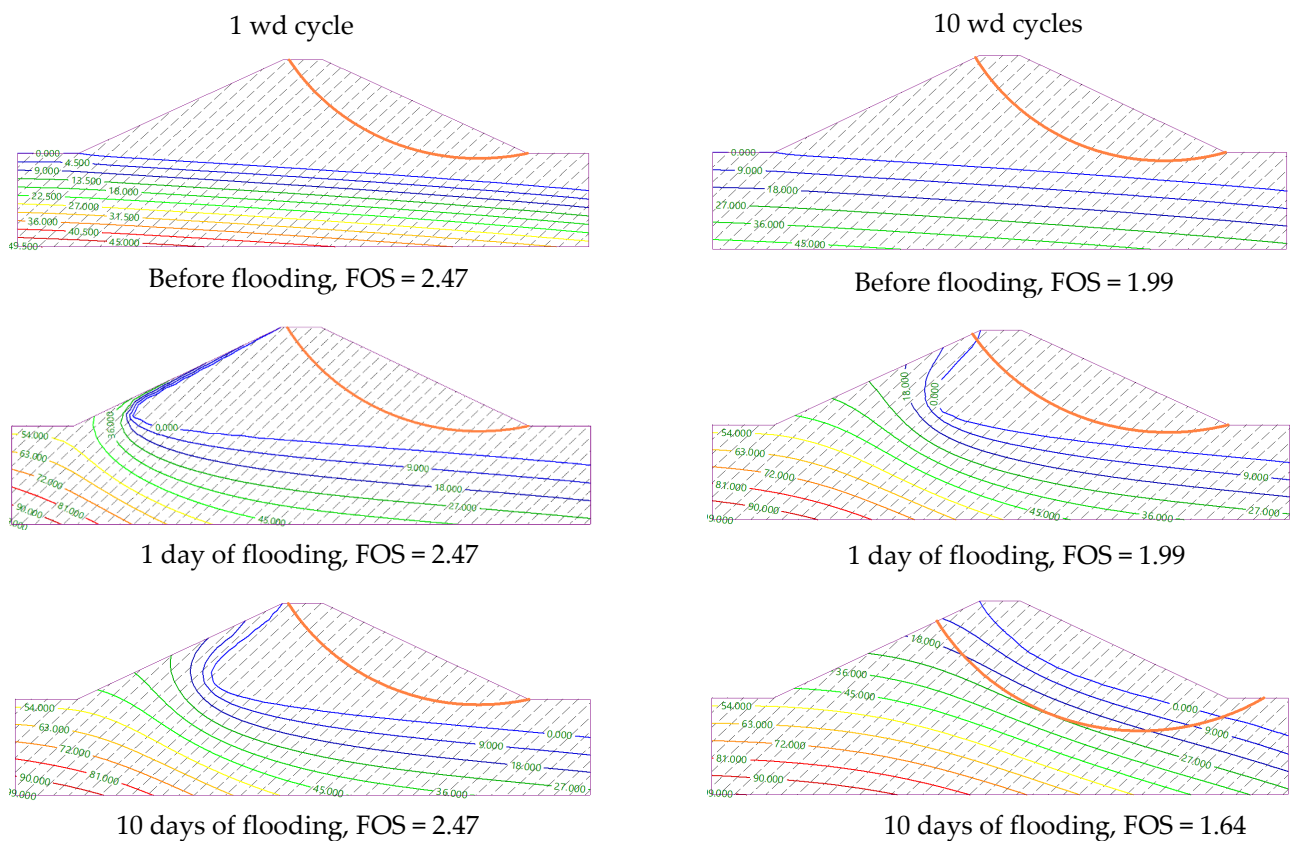| Type	Condition	Flooding Time (Days)	Inflow (m³/m/Day)	Outflow (m³/m/Day)	Difference (m³/m/Day)	Factor of Safety
Clay embankment	0 wd—new embankment	0	0.001	0.001	0	2.47
		1	0.225	0.001	0.224	2.47
		5	0.127	0.001	0.126	2.47
		10	0.127	0.001	0.126	2.47
Clay embankment	10 wd—aged embankment	0	0.005	0.001	0.004	1.99
		1	0.749	0.006	0.743	1.99
		5	0.754	0.006	0.748	1.72
		10	0.756	0.006	0.750	1.64
Silty sand embankment	0 wd—new embankment	0	0.177	0.177	0	1.68
		1	4.777	0.529	4.248	1.68
		5	2.786	2.062	0.724	1.23
		10	2.539	2.462	0.077	1.06
Silty sand embankment	10 wd—aged embankment	0	0.171	0.171	0	1.84
		1	4.614	0.528	4.086	1.84
		5	2.775	1.873	0.902	1.33
		10	2.554	2.306	0.248	1.15

Figure 8. Stability of a flood embankment built with clayey soil exposed to 1 and 10 wetting and drying cycles before flooding and at 1 and 10 days of flooding. Multicoloured lines represent pore water pressure profiles, and a thick orange line represents the failure surface.

The initial factor of safety for a recently constructed embankment composed of silty sand was determined to be 1.68. This value remained unchanged when the embankment experienced flooding at the crest level on day 1. However, after 5 days of flooding at

the crest level, the factor of safety decreased to 1.23 (Table 3). Subsequently, after 10 days of flooding, the embankment became fully saturated, reducing the factor of safety to 1.06, representing a 37% decrease in stability between dry and saturated conditions. This occurred due to the embankment reaching full saturation after 10 days of flooding, as the saturated hydraulic conductivity of silty sand is higher than that of clayey soil.

Following ten wetting and drying cycles, simulating an aged silty sand embankment, the factor of safety increased to 1.84, indicating a 10% improvement. This enhancement can be attributed to the consolidation and compaction of the silty sand soil resulting from the wetting and drying process. Notably, the impact of flooding on the silty sand embankment appears to be consistent, irrespective of whether the embankment is newly constructed or aged. The factor of safety of the aged embankment was found to be 1.84, 1.33, and 1.15 for 1, 5, and 10 days of flooding, respectively (Table 3 and Figure 9).
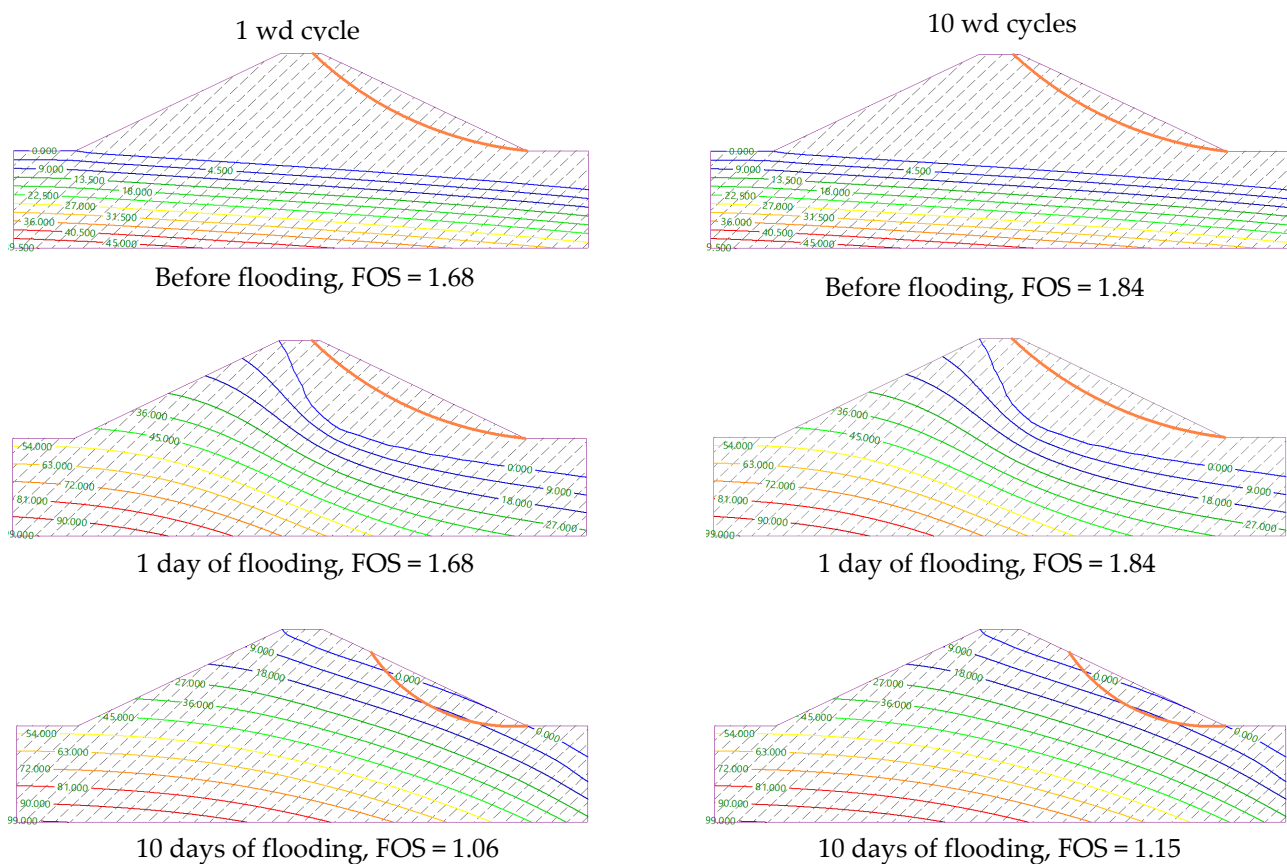

Figure 9. Stability of a flood embankment built with silty sand soil exposed to 1 and 10 wetting and drying (wd) cycles before flooding and at 1 and 10 days of flooding to the crest level. Multicoloured lines represent pore water pressure profiles, and a thick orange line represents the failure surface.

4. Discussion

The work presented in this paper provides evidence that cracking in clayey soil due to the action of wetting and drying [4] and the resultant loss of strength and water retention capacity, along with increased permeability, is a precursor to the initiation of progressive failure. In contrast, silty sand soil becomes compacted and consolidated with wetting and drying cycles, which improves its shear strength and slope stability.

The deterioration of the clay soil samples resulted from significant swelling and shrinkage during wetting and drying (wd) cycles, leading to permanent changes in the pore structure and crack formation. In contrast, silty sand soil showed considerably less shrinkage and swelling during wd cycles. Wetting gradually increased the number and size of intra- and inter-aggregate pores in clayey soil [33]. The evolution of the pore structure in

clayey soil during wetting is closely related to the wetting conditions. Under unconfined conditions, soil aggregates expanded and broke into smaller pieces, mainly increasing intra-aggregate pore sizes [34]. In confined wetting, inter-aggregate pores gradually closed, while intra-aggregate pores increased in volume [35,36]. On drying, the volume of clayey soil significantly decreased, primarily due to the significant shrinkage of macropores, while micropores remained unchanged or slightly increased in size [37]. Repeated wd cycles caused cumulative damage to the clayey soil, enlarging localised weak zones and developing cracks at the mesoscopic scale [38]. This is supported by Stirling et al. [14], who demonstrated that successive wetting and drying caused the development of a progressively increasing network of interconnected micro-scale cracks throughout soil specimens. Similar results were observed by Azizi et al. [39] when compacted silty clay was exposed to six wetting and drying cycles.

Due to 10 wd cycles, the increasingly porous clayey soil lost the ability to generate the same magnitude of suction at a given water content, compared to the clayey soil's soil water characteristic curve at 1 wd cycle. Wetting and drying cycles caused a shift in the soil water characteristic curve for clayey soil, as demonstrated in Figure 5, but when wetting and drying cycles continued over the same suction range, the movement in the curves stopped after 3–4 cycles [40,41]. The soil water retention behaviour then became quite repeatable. However, Stirling et al. [14] showed that if a sample is subject to wetting and drying cycles where the suction is increased beyond that experienced before, the wetting and drying loop shifts downwards. This means that each time drying progresses beyond the prior maximum suction value that an asset has been subject to, because of a more extreme drying event than has occurred in its history, an additional deterioration in performance due to suction loss can be expected. The saturated hydraulic conductivity of clayey soil treated with 10 wetting and drying cycles was measured about 5 times higher than that after 1 wetting and drying cycle. Supporting this, Stirling et al. [14] found a clear connectivity between cracking and near-surface saturation and run-off. Similar results were reported by Dixon et al. [42]. They found large variability in hydraulic conductivity in the uppermost 1 m of a clayey embankment, with values in the top 0.8 m having a range from 1×10^{-4} to 5×10^{-10} m/s (i.e., over five orders of magnitude) and a marked reduction in hydraulic conductivity with depth. Therefore, exposure to weather-driven deterioration affects the near-surface zone of clayey soil, which reduces soil water retention and increases hydraulic conductivity. However, no significant difference in the soil water characteristic curves was found for silty sand soil between 1 and 10 wetting and drying cycles (Figure 5). The saturated hydraulic conductivity for the silty sand soil was reduced by 3% at 10 wd cycles compared to 1 wd cycle (Table 1).

Understanding the effective shear strength of soil is crucial for evaluating the long-term stability of foundations, slopes, and other engineering projects, predicting future stability, and issuing safety warnings. Our research found that the effective angle of internal friction in clayey soil significantly decreased with more wetting and drying cycles, while the effective cohesion remained relatively unchanged. There is limited research on the drained/effective shear strength of soil influenced by wetting and drying cycles, and existing studies show conflicting results. For example, Zhou et al. [38] found that the internal friction angle fluctuates within a narrow range, with the reduction in cohesion being the primary cause of shear strength degradation during wd cycles. Zhu et al. [43] and Khan et al. [9] reported a decrease in both the cohesion and the internal friction angle of soil with additional wd cycles for expansive soils. Hafhouf et al. [44] observed a significant reduction in cohesion but an increase in the internal friction angle of Sebkha soil with additional wd cycles.

The increase in the angle of internal friction for silty sand from 1 to 10 wetting and drying (wd) cycles can be attributed to several factors related to the soil structure, particle rearrangement, and compaction effects. Initially, silty sand may have a relatively loose structure with more void spaces. As the soil undergoes multiple wd cycles, the particles tend to settle and rearrange more tightly, reducing void spaces and increasing the soil's

density. These cycles lead to particle rearrangement, which densifies the soil structure, reducing void spaces and enhancing interparticle friction [21]. Additionally, changes in soil suction during these cycles cause particles to draw closer together, further stabilising the soil. Studies by Nahlawi and Kodikara [45] and Rahardjo et al. [46] supported these findings, showing increased soil strength and particle interlocking with repeated wd cycles.

A loss of suction at a given water content, a high saturated hydraulic conductivity, crack formation in soils, and, hence, a reduction in shear strength are significant problems in earth-based infrastructure [47,48]. Shrinkage cracks can cause severe damage to the serviceability of earth-based infrastructure. There is evidence that cracks in slopes can penetrate to a depth of approximately 1 m [47,48] and that a hydrologically distinct layer exists in the top 1.5 m of a clayey slope [49]. In recent years, significant effort has been directed to better analyse ground and climate interactions applicable to a range of earth-based structures [14]. Comparing the two soil types, it is evident from our study that clayey soil embankments initially possess higher stability, as indicated by their higher safety factor (FOS). However, the stability of clayey soil is more adversely affected by wd cycles and prolonged flooding, showing a more significant decline in its FOS over time. The weathering process in clay is partly a combination of cracking (and the resultant enhanced surface hydraulic conductivity) and a loss of strength due to a reduced ability to generate and maintain suction. This reduction in shear strength can cause down-slope movements, which, if large enough, can result in strain softening and load redistribution. Ultimately, changes in loading or further weather-driven deterioration could lead to slope failure. On the other hand, silty sand soil exhibits lower initial stability but shows greater resilience to wd cycles. Despite this, its FOS declines under prolonged flooding due to the high saturated hydraulic conductivity. This suggests that while silty sand resists wd cycle-related deterioration, its stability is compromised due to increased pore water pressure and reduced effective stress due to prolonged flooding.

5. Conclusions

This laboratory study examined the effects of wetting and drying cycles on the hydromechanical properties of clayey and silty sand soils. The findings indicated a significant degradation in clayey soil, in contrast to the more resilient response exhibited by silty sand. The deterioration observed in clayey soil is primarily associated with microstructural changes within its fabric, which lead to a diminished capacity for generating and sustaining suction. These alterations at the microstructural level result in macrostructural implications, including an increase in saturated hydraulic conductivity and a notable decrease in shear strength.

Conversely, silty sand soil demonstrated enhanced resilience to wetting and drying cycles, characterised by less pronounced shrinkage and swelling. The increase in the angle of internal friction in silty sand during repeated wetting and drying can be ascribed to particle rearrangement, densification, and improved interparticle friction.

The factor of safety of the clayey embankment significantly decreased because of exposure to wetting and drying cycles. In contrast, a slight increase in the factor of safety was observed for the silty sand embankment due to wetting and drying cycles. The impact of the flooding duration was notably more pronounced on the silty sand embankment than the clayey embankment due to its relatively permeable nature. The clay embankment exhibited impervious behaviour, with minimal inflow and outflow recorded and no seepage observed during the 10-day flooding period. In contrast, the silty sand embankment facilitated rapid water infiltration, achieving steady-state conditions by the conclusion of the 10-day flooding period, along with considerable seepage.

The implications of this research hold promise for enhancing predictive capabilities regarding deteriorating conditions and emerging failures, enabling asset owners to make informed investments in proactive remediation strategies. This approach may mitigate unforeseen failures, strengthen assets' resilience against climate change, and significantly reduce the associated economic impacts.

References

1. European Environment Agency. *Climate Change Adaptation and Disaster Risk Reduction in Europe*; European Environment Agency, Publications Office of the European Union: Luxembourg, 2017.
2. Clarke, D.; Smethurst, J.A. Effects of climate change on wetting and drying cycles in engineered clay slopes in England. *Q. J. Eng. Geol. Hydrogeol.* **2010**, *43*, 473–486. [CrossRef] [PubMed]
3. Tang, C.S.; Wang, D.Y.; Shi, B.; Li, J. Effect of wetting–drying cycles on profile mechanical behaviour of soils with different initial conditions. *Catena* **2016**, *139*, 105–116.
4. Turrakheil, K.S.; Shah, S.S.A.; Naveed, M. Evolution of Soil Pore Structure and Shear Strength Deterioration of Compacted Soil under Controlled Wetting and Drying Cycles. *Atmosphere* **2024**, *15*, 843. [CrossRef]
5. Xu, B.; Yin, Z.; Liu, S.-L. Experimental study of the factors and laws affecting the strength of expansive soil. *Rock Soil Mech.* **2011**, *32*, 44–50.
6. Li, X.Y.; Hu, H.B.; Guo, W. Dry-wet circulation intensity attenuation law of subgrade under the condition of clay. *Highw. Eng.* **2014**, *164*, 150–152.
7. Xu, J.; Zhou, L.; Hu, K.; Li, Y.; Zhou, X.; Wang, S. Influence of wet-dry cycles on uniaxial compression behaviour of fissured loess disturbed by vibratory loads. *KSCE J. Civ. Eng.* **2022**, *26*, 2139–2152. [CrossRef]
8. Niu, Z.L.; Xu, J.; Li, Y.F.; Wang, Z.F.; Wang, B. Strength deterioration mechanism of bentonite modified loess after wetting–drying cycles. *Sci. Rep.* **2022**, *12*, 3130. [CrossRef]
9. Khan, M.A.; Hossain, M.S.; Khan, M.S.; Samir, S.; Aramoon, A. Impact of wet-dry cycles on the shear strength of high plastic clay based on direct shear testing. In Proceedings of the Geotechnical Frontiers 2017, Orlando, FL, USA, 12–15 March 2017; pp. 615–622.
10. Zhang, J.R.; Xu, Q.; Sun, D.A. Simulation of soil-water characteristic curves during drying and wetting cycles. *Rock Soil Mech.* **2014**, *35*, 689–695.
11. Dyer, M. Performance of flood embankments in England and Wales. In Proceedings of the Institution of Civil Engineers-Water Management; Thomas Telford Ltd.: London, UK, 2004; Volume 157, pp. 177–186.
12. Gowthaman, S.; Nakashima, K.; Kawasaki, S. Effect of wetting and drying cycles on the durability of biocemented soil of expressway slope. *Int. J. Environ. Sci. Technol.* **2022**, *19*, 2309–2322. [CrossRef]
13. Rasul, J.M.; Ghataora, G.S.; Burrow, M.P. The effect of wetting and drying on the performance of stabilised subgrade soils. *Transp. Geotech.* **2018**, *14*, 1–7. [CrossRef]
14. Stirling, R.A.; Toll, D.G.; Glendinning, S.; Helm, P.R.; Yildiz, A.; Hughes, P.N.; Asquith, J.D. Weather-driven deterioration processes affecting the performance of embankment slopes. *Géotechnique* **2021**, *71*, 957–969. [CrossRef]
15. Tu, Y.; Zhang, R.; Zhong, Z.; Chai, H. The strength behavior and desiccation crack development of silty clay subjected to wetting-drying cycles. *Front. Earth Sci.* **2022**, *10*, 852820. [CrossRef]
16. Zhao, G.T.; Han, Z.; Zou, W.L.; Wang, X.Q. Evolution of mechanical behaviours of an expansive soil during drying-wetting, freeze-thaw, and drying-wetting-freeze–thaw cycles. *Bull. Eng. Geol. Environ.* **2021**, *80*, 8109–8121. [CrossRef]
17. Zhang, J.; Hu, H.; Peng, J.; Zhang, Y.; Zhang, A. Enhanced understanding of subgrade soil hydraulic characteristics: Effects of wetting–drying cycles and stress states on subgrade water migration. *J. Hydrol.* **2024**, *635*, 131165. [CrossRef]
18. Ng, C.; Daniel, P. Pore structure effects on the water retention behaviour of a compacted silty sand soil subjected to drying-wetting cycles. *Eng. Geol.* **2023**, *313*, 106963. [CrossRef]
19. Jing, J.; Hou, J.; Sun, W.; Chen, G.; Ma, Y.; Ji, G. Study on influencing factors of unsaturated loess slope stability under dry-wet cycle conditions. *J. Hydrol.* **2022**, *612*, 128187. [CrossRef]

20. Wen, T.; Chen, X.; Shao, L. Effect of multiple wetting and drying cycles on the macropore structure of granite residual soil. *J. Hydrol.* **2022**, *614*, 128583. [CrossRef]

21. Chen, X.; Quan, Q.; Zhang, K.; Wei, J. Spatiotemporal characteristics and attribution of dry/wet conditions in the Weihe River Basin within a typical monsoon transition zone of East Asia over the recent 547 years. *Environ. Model. Softw.* **2021**, *143*, 105116. [CrossRef]

22. Ventini, R.; Dodaro, E.; Pirone, M.; Giretti, D.; Gragnano, C.G.; Fioravante, V.; Gottardi, G.; Mancuso, C. Integrated Physical and Numerical Modelling to Study the Hydro-Mechanical Response of a River Embankment. In *National Conference of the Researchers of Geotechnical Engineering*; Springer Nature: Cham, Switzerland, 2023; pp. 569–577.

23. Zhao, Y. The Influence of Rainfall and Evaporization Wetting-Drying Cycles on the Slope Stability. In *Advances in Meteorology*; Wiley: Hoboken, NJ, USA, 2022; pp. 1–8. [CrossRef]

24. Hassan, M.A.; Ismail, M.A.M.; Shaalan, H.H. Numerical modelling for the effect of soil type on stability of embankment. *Civ. Eng. J.* **2022**, *7*, 41–57. [CrossRef]

25. *BS 1377-1: 2016*; Methods of Test for Soils for Civil Engineering Purposes–Part 1: General Requirements and Sample Preparation. The British Standards Institution: London, UK, 2016.

26. *BS 1377-2: 2022*; Methods of Test for Soils for Civil Engineering Purposes—Part 2: Classification Tests and Determination of Geotechnical Properties. The British Standards Institution: London, UK, 2016.

27. *BS 1377-4: 1990*; Methods of Test for Soils for Civil Engineering Purposes–Compaction Related Tests. The British Standards Institution: London, UK, 1990.

28. *BS 1377-6: 1990*; Methods of Test for Soils for Civil Engineering Purposes. Consolidation and Permeability Tests in Hydraulic Cells and with Pore Pressure Measurement. The British Standards Institution: London, UK, 1990.

29. *ASTM Standard D5298-03*; Standard Test Method for Measurement of Soil Potential (Suction) Using Filter Paper. ASTM International: West Conshohocken, PA, USA, 2017.

30. Chandler, R.J.; Crilly, M.S.; Montgomery-Smith, G. A low-cost method of assessing clay desiccation for low-rise-buildings. *Proc. Inst. Civ. Eng.* **1992**, *92*, 82–89. [CrossRef]

31. Van Genuchten, M.T. A closed-form equation for predicting the hydraulic conductivity of unsaturated soils. *Soil Sci. Soc. Am. J.* **1980**, *44*, 892–898. [CrossRef]

32. Shah, S.S.A.; Asif, A.R.; Ahmed, W.; Islam, I.; Waseem, M.; Janjuhah, H.T.; Kontakiotis, G. Determination of Dynamic Properties of Fine-Grained Soils at High Cyclic Strains. *Geosciences* **2023**, *13*, 204. [CrossRef]

33. Tang, C.-S.; Cheng, Q.; Gong, X.; Shi, B.; Inyang, H.I. Investigation on microstructure evolution of clayey soils: A review focusing on wetting/drying process. *J. Rock Mech. Geotech. Eng.* **2023**, *15*, 269–284. [CrossRef]

34. Ye, W.M.; Wan, M.; Chen, B.; Cui, Y.; Wang, J. Micro-structural behaviors of densely compacted GMZ01 bentonite under drying/wetting cycles. *Chin. J. Geotech. Eng.* **2011**, *33*, 1173–1177.

35. Cui, Y.J.; Yahia-Aissa, M.; Delage, P. A model for the volume change behavior of heavily compacted swelling clays. *Eng. Geol.* **2002**, *64*, 233–250. [CrossRef]

36. Liu, Y. Investigation on the swelling properties and microstructure mechanism of compacted Gaomiaozi bentonite. *J. Eng. Geol.* **2016**, *24*, 451–458.

37. Cuisinier, O.; Auriol, J.C.; Le Borgne, T.; Deneele, D. Microstructure and hydraulic conductivity of a compacted lime-treated soil. *Eng. Geol.* **2011**, *123*, 187–193. [CrossRef]

38. Zhou, R.; Wang, B.; Han, S.; Wang, D.; Zhang, F. Mechanisms of crack development and strength deterioration in compacted expansive soils under controlled wetting-drying conditions. *Eng. Fail. Anal.* **2024**, *159*, 108133. [CrossRef]

39. Azizi, A.; Musso, G.; Jommi, C. Effects of repeated hydraulic loads on microstructure and hydraulic behaviour of a compacted clayey silt. *Can. Geotech. J.* **2019**, *57*, 100–114. [CrossRef]

40. Alonso, E.E.; Romero, E.; Hoffmann, C.; García-Escudero, E. Expansive bentonite-sand mixtures in cyclic controlled suction drying and wetting. *Eng. Geol.* **2005**, *81*, 213–226. [CrossRef]

41. Liu, G.; Toll, D.G.; Kong, L.; Asquith, J.D. Matric suction and volume characteristics of compacted clay soil under drying and wetting cycles. *Geotech. Test. J.* **2020**, *43*, 20170310. [CrossRef]

42. Dixon, N.; Crosby, C.J.; Stirling, R.; Hughes, P.N.; Smethurst, J.; Briggs, K.; Hughes, D.; Gunn, D.; Hobbs, P.; Loveridge, F.; et al. In situ measurements of near-surface hydraulic conductivity in engineered clay slopes. *Q. J. Eng Geol. Hydrogeol.* **2019**, *52*, 123–135. [CrossRef]

43. Zhu, R.; Cai, Z.; Huang, Y.; Zhang, C.; Guo, W.; Wang, Y. Effects of wetting-drying-freezing-thawing cycles on mechanical behaviours of expansive soil. *Cold Reg. Sci. Technol.* **2022**, *193*, 103422. [CrossRef]

44. Hafhouf, I.; Khelifa, A. Impact of drying-wetting cycles on shear properties, suction, and collapse of Sebkha soils. *Heliyon* **2023**, *9*, e13594. [CrossRef]

45. Nahlawi, H.; Kodikara, J. Laboratory Experiments on Desiccation Cracking of Thin Soil Layers. *Geotech. Geol. Eng.* **2006**, *24*, 1641–1664. [CrossRef]

46. Rahardjo, H.; Leong, E.C.; Rezaur, R.B. Effect of antecedent rainfall on pore-water pressure distribution characteristics in residual soil slopes. *J. Hydrol.* **2004**, *287*, 24–42.

47. Anderson, M.G.; Hubbard, M.G.; Kneale, P.E. The influence of shrinkage cracks on pore-water pressures within a clay embankment. *Q. J. Engng Geol. Hydrogeol.* **1982**, *15*, 9–14. [CrossRef]

48. Dyer, M.; Utili, S.; Zielinski, M. Field survey of desiccation fissuring of flood embankments. *Proc. Instn Civ. Engrs–Wat. Manag.* **2009**, *162*, 221–232. [CrossRef]
49. Ng, C.W.W.; Zhan, L.T.; Bao, C.G.; Fredlund, D.G.; Gong, B.W. Performance of an unsaturated expansive soil slope subjected to artificial rainfall infiltration. *Géotechnique* **2003**, *53*, 143–157. [CrossRef]